

Document downloaded from:

<http://hdl.handle.net/10251/124215>

This paper must be cited as:

Ocaña-Levario, S.J.; Carreño-Alvarado, E.P.; Ayala Cabrera, D.; Izquierdo Sebastián, J. (2018). GPR image analysis to locate water leaks from buried pipes by applying variance filters. *Journal of Applied Geophysics*. 152:236-247.
<https://doi.org/10.1016/j.jappgeo.2018.03.025>



The final publication is available at

<http://doi.org/10.1016/j.jappgeo.2018.03.025>

Copyright Elsevier

Additional Information

GPR image analysis to locate water leaks from buried pipes by applying variance filters

**Silvia J. Ocaña-Levario¹, Elizabeth P. Carreño-Alvarado¹, David Ayala-Cabrera²
and Joaquín Izquierdo¹**

¹ Universitat Politècnica de València
Camino de Vera s/n, Valencia, 46022, España
e-mail: silocle@upv.es, elcaral@upv.es, jizquier@upv.es

² Irstea, UR ETBX, Dept. of Water, France,
david.ayala@irstea.fr

ABSTRACT

Nowadays, there is growing interest in controlling and reducing the amount of water lost through leakage in water supply systems (WSSs). Leakage is, in fact, one of the biggest problems faced by the managers of these utilities. This work addresses the problem of leakage in WSSs by using GPR (Ground Penetrating Radar) as a non-destructive method. The main objective is to identify and extract features from GPR images such as leaks and components in a controlled laboratory condition by a methodology based on second order statistical parameters and, using the obtained features, to create 3D models that allows quick visualization of components and leaks in WSSs from GPR image analysis and subsequent interpretation. This methodology has been used before in other fields and provided promising results. The results obtained with the proposed methodology are presented, analyzed, interpreted and compared with the results obtained by using a well-established multi-agent based methodology. These results show that the variance filter is capable of highlighting the characteristics of components and anomalies, in an intuitive manner, which can be identified by non-highly qualified personnel, using the 3D models we develop. This research intends to pave the way towards future intelligent detection systems that enable the automatic detection of leaks in WSSs.

Keywords: Variance filters, GPR images, non-destructive methods, water leaks, water supply systems

1. INTRODUCTION

In the last years, water leaks have taken a leading role in the management of urban water supply systems (WSSs) because leakage represents a serious problem that severely affects WSS utilities and, ultimately, water consumers. According to several reports, a substantial amount of water gets lost through leaks in WSSs (Martini et al., 2015; Nasirian et al., 2013). For example, the World Bank in partnership with the International Water Association states that in developing countries, in a coarse manner, 45 million cubic meters of water are lost daily. This, in economic terms, can be valued over US\$3 billion per year. This amount decreases in more developed countries (World Bank, 2016). To face this problem, it is crucial to implement actions to detect, locate and control leaks in water networks.

Leaks in WSSs not only represent a high percentage of quality water loss, but also reduce system efficiency, put water quality at risk, and produce economic cost increase for the utility. To overcome efficiently this problem, early detection of anomalies and precise location of the flaws are deemed necessary. To serve this purpose, the most common methods are the acoustic method (Brennan et al., 2008; Hunaidi et al., 2004; Juliano et al., 2013), infrared thermography (Atef et al., 2016; Fahmy and Moselhi, 2010), gas trace test and ground penetrating radar (GPR) (Demerci et al., 2012; Dong et al., 2011; Lee and Oh, 2018). Among them, GPR is one of the most effective tools for the characterization of ground conditions in urban areas (Hong et al. 2018), thus, in particular, making it easier water network inspection by demarking in GPR images (radargrams) contrasts between leaked water and the surrounding ground derived from their dielectric characteristics (Crocco et al., 2010). This is the reason why, in the last years, GPR use has been extended to various subsurface geophysical investigations, particularly at shallow depths (Shaikh et al. 2018; Lai et al., 2018). GPR is an easily applied and fast methodology; however, the images obtained are not easy to interpret (Ayala-Cabrera et al., 2011; Gerlitz et al., 1993; Thomson et al. 2009). It is necessary an adequate treatment of the images by applying different processes and filters (Santos and Teixeira, 2017; Xue et al., 2017) that help the visualization of the sought characteristics (buried pipes and water leaks, in our case). Accordingly, works such as Stampolidis et al. (2003), use GPR image processing by low-band filters to identify leaks in PVC urban pipelines; Hasan (2012) and Hyun et al. (2007) perform background extraction and image filtering of GPR images, respectively; furthermore, Simi et al. (2008) uses the Hough transform to locate hyperbolas in GPR images; Tavera (2008) uses the Hilbert and Fourier transforms; and Ayala-Cabrera et al. (2011) applies a multi-agent methodology for similar purposes, just to name a few. All of them show varied efficiency for locating buried objects and specific damages in networks by applying adequate processing methodologies to GPR images.

However, most of these works are based only on the location and interpretation of the hyperbolas generated either in raw or pre-processed images. For that reason, this work focus on the evaluation of the viability of identifying and extracting morphological characteristics (contours, patterns, etc.) corresponding to a water leak from a PVC pipe under laboratory controlled conditions. In this framework, recent laboratory assays and water leak image processing contributions, such as Lai et al. (2016) on GPR image pattern detection, or Ocaña-Levario et al. (2015) and Ayala-Cabrera et al. (2013a) by using Multi-Agent-Based Simulation (MABS) for GPR image pre-processing, can be quoted. In this work, the proposed methodology uses second order statistical (variance filter) parameters to highlight features of interest, such as, objects (pipes) and leaks, which help improve their posterior feature extraction. Enhanced visualization is obtained from more differentiated contrasts, which, in addition, is independent of the direction of the prospection with respect to the location of the element of interest. These advantages are highlighted after comparison with the MABS methodology, a well-established visualization technique. The main objective of this process is to extract leak characteristics from GPR images using a variance filter, and then create 3D models for better understanding WSS buried elements. In future works we expect to use the variance filter-extracted characteristics as inputs for intelligent detection systems, allowing automatic leak detection, and ultimately, to improve efficiency in urban water management.

Related to the employed approach in this document, we have to quote recent researches like Fabijariska (2011), which uses a variance filter to determine contour locations in synthetic

and real images, and Sarwas and Skoneczny (2015), which tries various variance filters to locate objects in RGB images. These two investigations show a promising use of variance filters, which are evaluated as a simple filter in RGB images.

In this work we prove that the variance filter overcomes the traditional scope based in boundary detection on GPR images, in a manner that the hyperbolas that are shown in GPR images as components can now be shown with differentiated shapes in the results obtained. As a consequence, it can be concluded that variance filters help the identification of WSS components and leaks, thus allowing the detection of contrasts between the various material borders within an image.

This paper is organized as follows. In the first section, we have presented a brief introduction to the subject and reviewed relevant literature. The second section is dedicated to the characteristics of the tests performed. The third section shows the proposed methodology based on a variance filter. The analysis and results of processed GPR images with the variance filter are presented in the fourth section. Next, the fifth section presents a comparison analysis between the results obtained by the proposed methodology (variance filter) and the results obtained by a multi-agent based system. The sixth section presents 3D models obtained by both methods to ease interpretation. Finally, a section of conclusions closes the document.

2. CASE STUDY – ASSAY CONFIGURATION

In this section, the laboratory assay configuration used to obtain the GPR images is presented. The proposed assay configuration is presented in Figure 2.1.

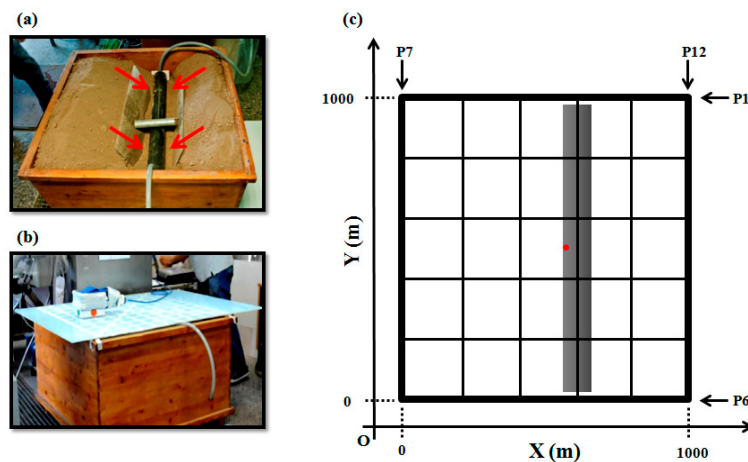


Figure 2.1. Assay configuration: (a) Buried pipe (black), (b) polypropylene plate (light blue) - GPR antenna of 1.5 GHz, (c) data sampling configuration

For the ensemble of tests, a 1.00×1.00×0.60-meter wooden tank was employed, thus emulating a land plot. Inside the tank a 0.95-meter-long and 0.10-meter diameter PVC pipe was buried in dry soil. It is important to say that the pipe was connected on both ends by two hose pieces, allowing introduction and extraction of water in and out of the system. Finally, to simulate a pipe break, the PVC pipe was drilled in the center. The pipe was covered with dry soil once placed inside the tank. On top of the tank a polypropylene plate was placed to

improve data acquisition. This configuration had also been used in other laboratory tests (Ayala-Cabrera et al.; 2013a; Ocaña-Levario, 2014) employing various pipe materials. It is worth mentioning that in both cases the location of the leak was inferred after a hard work of interpretation developed by experts in image analysis. The plate had 12 traces (slices), 6 parallel to the X axis (P1 to P6) and 6 parallel to the Y axis (P7 to P12), equally spaced, with separation 0.20 meters, thus producing a sampling mesh in which the GPR antenna was slid to capture data. This configuration was intended to ease the fieldwork of operators in capturing the information.

The GPR equipment used for the assays corresponds to a 1.5 GHz central frequency monostatic antenna, with parameters 120 traces/s, 512 data/trace and 20 ns/512 data. The antenna selection was performed given the required soil penetration characteristics, taking also into consideration the shallowness of real pipelines buried in water supply systems (Ayala-Cabrera et al., 2013b).

Additionally, to compare between normal operation conditions of the pipe and a leakage condition, this work proposes two scenarios. The first scenario was performed without water inside the pipe (no leak case); in the second scenario, the pipe was filled with water, which was leaking through the drilled hole.

3. PROPOSED METHODOLOGY – VARIANCE FILTER

The proposed methodology for leak boundary identification and extraction from GPR images is presented in this section. First the variance filter is introduced, then the methodology applied to the images is described.

Variance filter. The basic principle of the *variance filter* consists in calculating the variance around each pixel of the image with size $m \times n$, m being the number of rows in the image and n the number of columns; this notation is used throughout this document. First, the window size $s \times o$ (number of pixels to work with) is defined. Then, an iterative process starts, which uses the variance filter formulation described by (Fabijańska, 2011):

$$\bar{u}_{ij} = \frac{1}{n} \sum_{i=1}^n u_{ij}; \quad (1)$$

$$\sigma_{ij}^2 = \frac{1}{n} \sum_{i=1}^n (u_{ij} - \bar{u}_{ij})^2. \quad (2)$$

In each step, the mean is first estimated for the chosen window. This mean is defined by equation (1), which uses the size of our window and the pixel values of the image. Next, the variance, is calculated by (2), with the pixels inside the selected window and the value obtained in equation (1); the result is associated to the center pixel of the window in the new image; this is repeated for all pixels of the image. By doing this, a new image is obtained. Notice that the new image is of size $(m-(s-1)) \times (n-(o-1))$.

The proposed methodology for leak boundary identification and extraction from GPR images is presented in this section. Figure 3.1 shows the process, which consists of the following steps: a) get the raw input image, b) apply the variance filter to obtained GPR images, c) smooth the filtered images, d) identify range objects of interest by binarization, and e) obtain the contour of the selected groups. Next, this methodology is concisely described.

Afterwards, in section six we explain how relevant patterns are extracted to create a 3D model.

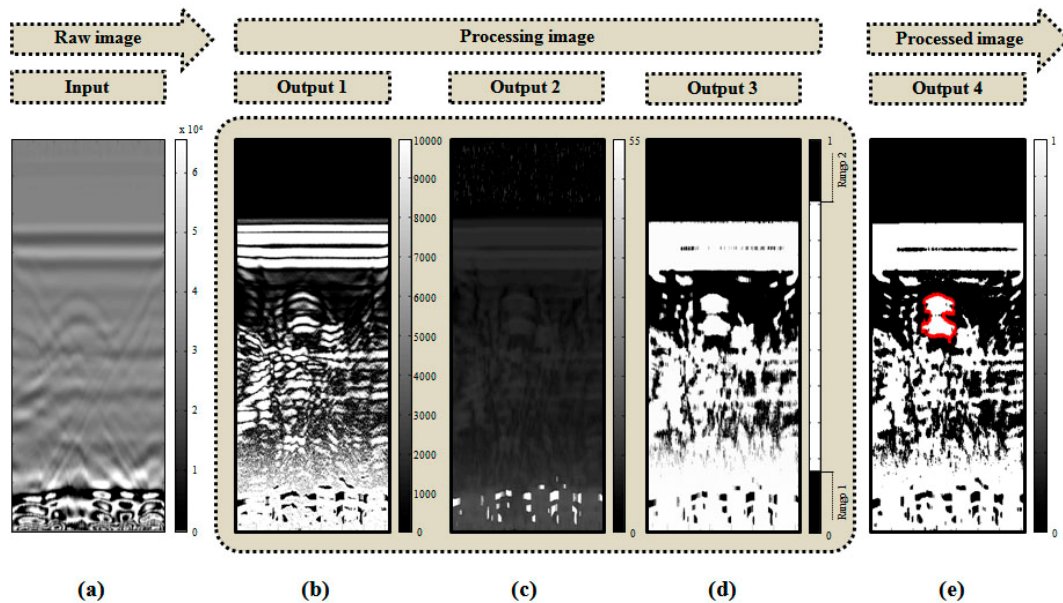


Figure 3.1 Methodology: (a) Raw input image, (b) variance filter image, (c) smoothed image, (d) binarized image and (e) processed image

Raw image. Is the GPR image obtained from laboratory surveys that will be used as input for the successive process.

Variance filter image. The variance filter is applied to the raw image. In our case, the window size proposed is 3×1 . At this point, it is important to note that the window size was selected after having performed several tests with different configurations. After having tried window sizes of 5×5 , 4×4 , 3×3 , 3×2 , 5×1 , 4×1 , and 3×1 , in 3 different images, the window size of 3×1 resulted the configuration that better improves image visualization while avoiding over-smoothing. In the next step, the variance filter image is processed for a visual analysis, to discover characteristics that give relevant information related to pipe location and/or leak.

Smoothed image. Noise from the variance filtering process in variance filter image is removed by using the median filter implemented in Matlab's function *medfilt1* (Matlab, 2012; Pratt, 2007). The function *medfilt1* applies an n -th order one-dimensional median filter to each row of the image. The application of this function helps thresholding the image and also highlights the area of interest. Once cleaned the image noise (Belotti et al. 2002; Harrison, 2005; Nagashree et al., 2014; Singh and Nene, 2013), we obtain a smoothed image.

Binarization. Over the smoothed image, an iterative segmentation is done, based on the selection of one or more ranges ([min max]). Ranges are selected manually by choosing the minimum and maximum values that enhance visualization and selection of the characteristics of the objects as well as the anomalies. As a result of the selection of ranges, a binarized matrix is obtained. The smoothed and binarized images have the same dimensions.

Processed image (contour selection). In the binarized image, boundary detection is obtained using the Moore's neighbor algorithm modified by Jacob Eliosoff (González, 2004). This algorithm is implemented in Matlab's *bwboundaries* function (Matlab, 2012). The *bwboundaries* function traces the exterior boundaries of objects, as well as boundaries of holes inside these objects, in the binarized image. Next, the selected contours for the images in both scenarios are compared; this results in an easy way to identify the boundaries belonging to the pipe and those belonging to the wet area created by the leak.

4. ANALYSIS OF RESULTS – VARIANCE FILTER

In this section, the results after applying the proposed methodology, as well as their interpretation, are shown. It is important to say that in this section the word *slice* is used to denote the GPR images, as they are sections in depth of the inspected ground. The GPR images are named transversal slices if the image was obtained from a prospection transversal to the pipe. Similarly, for longitudinal GPR inspections we speak of longitudinal slices. First, we show the transversal slices for the first scenario, followed by the longitudinal slices for the first scenario. Next, for the second scenario both transversal and longitudinal slices, in this order, are also shown.

4.1. First scenario – Transversal slices

Figure 4.1a shows raw slices; there is evident difficulty to locate characteristics that confirm the presence of some object or anomaly; nevertheless, by analyzing the slices in detail, the hyperbolas obtained after moving the antenna transversally to the buried pipe can be identified. Hyperbolas are found between 200 and 250 samples (depth) showing the presence of the pipe. The raw images show diagonal lines crossing through and intersecting in the middle of each image approximately; these lines are signal reflections created by the tank walls, generating noise on the images. In slice P4 a couple of additional hyperbolas (anomalies) are shown. These anomalies can cause confusion in posterior analyses, since they could be mistaken for the leak if not considered in the starting analysis. These hyperbolas cannot be caused by the leak since no water has been introduced to the system yet (first scenario).

Figure 4.1b shows the slices obtained after the variance filtering process; curve-shaped ensembles that match the location of the hyperbolas in the raw images between 200 and 250 samples approximately can be observed. Also, in all of the images, around 175 samples a clear contrast in the images can be found; this contrast denotes the surface of the ground inside the tank. In slices P3 to P5 the shapes that appear in the images are very similar, having 3 to 4 curves that create a circular shape. This does not occur in slice P1 because of the hose that is connected to the pipe; the presence of this hose, which feeds the system with water, also affects slice P2 and slightly P6. It is important to mention that slice P4 still has the anomaly visible to the right of the ensemble of curves that are considered to be the pipe. Finally, Figure 4.1c shows the contour selection of the shapes in each image.

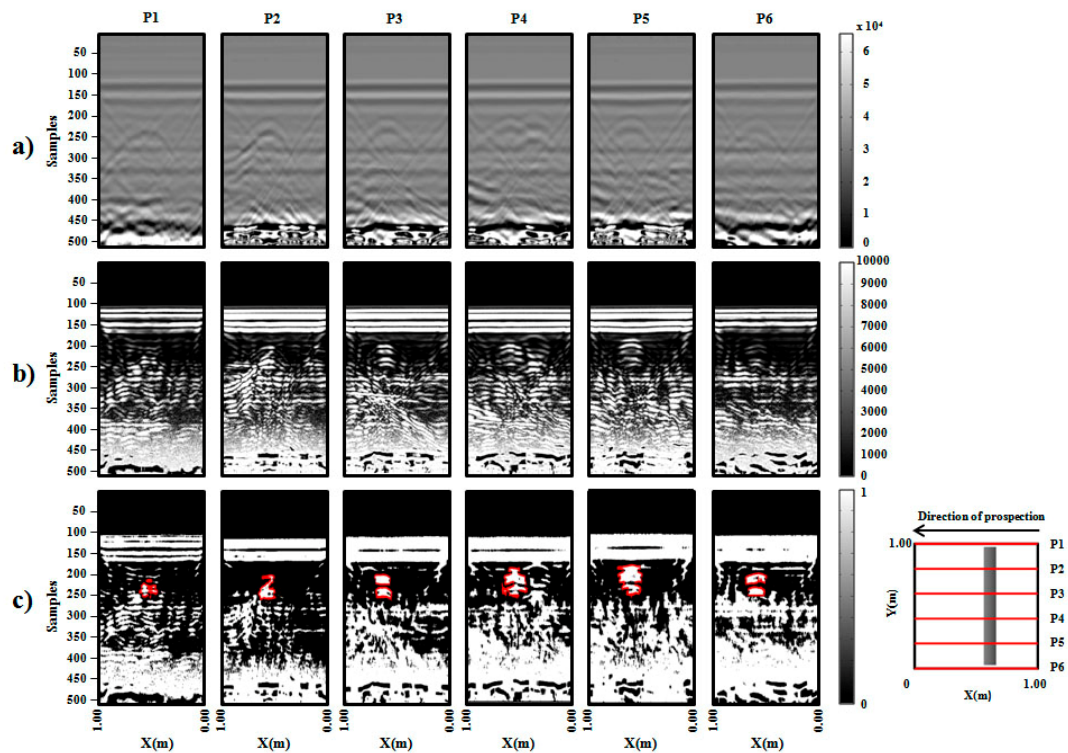


Figure 4.1 a) Raw images, b) variance filter images, and c) binarized images

4.2. First scenario – Longitudinal slices

In these images the longitudinal layout of the pipe is visible. Normally, experts first locate the pipe by looking for hyperbolas in transversal slices. However, in these images it is shown that it is possible to locate the pipe from longitudinal slices.

Figure 4.2a shows the raw images. In the slices the diagonal lines resulting from the reflected signal produced by the tank wall are visible, similar to the slices in figure 4.1a. Also, as in figure 4.1a, it is difficult to identify the presence of the pipe; however, when looking closely and comparing the slices, slice P4 shows a couple of parallel lines, which are demarked slightly; these lines correspond to the pipe located between 200 and 250 samples. In a prospection longitudinal to the buried pipe it is a harder task to find the pipe if compared to a prospection transversal to the pipe since no hyperbolas appear in the raw images; as in this case, the pipe is shown as various parallel lines, that can be easily mistaken or overlooked. Figure 4.2b shows the slices once finished the variance filter process; the presence of the pipe in slice P4, between 200 and 250 samples can be clearly seen. Pipe top and bottom boundaries are highlighted, being, then, easier to detect. Finally, figure 4.2c shows the binarized slices and the shapes selected. Only slice P4 has a shape to locate the pipe; in all the other slices there is nothing to remark.

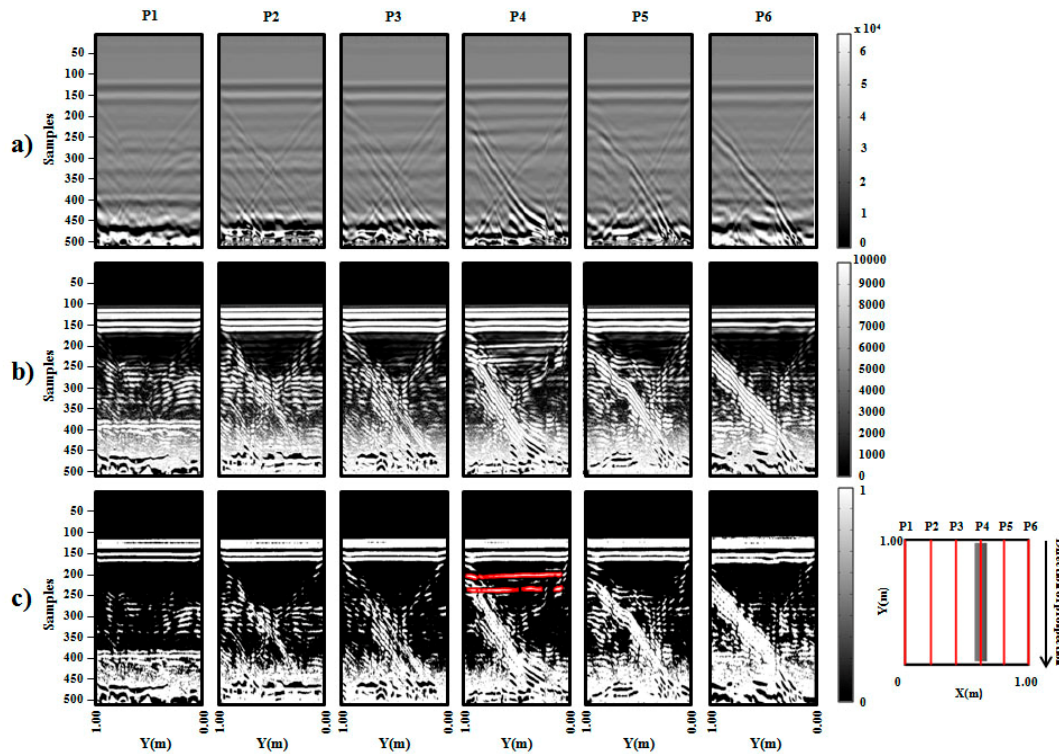


Figure 4.2 a) Raw image, b) variance filter images, and c) binarized images

4.3. Second scenario – Transversal slices

In Figure 4.3a the raw slices for the second scenario are shown. First, in slices P1 and P6 a vertical distortion caused by the water present in the system can be observed. In slice P1 this distortion is due to water entering the system and in P6 it is caused by water leaving the system. In slices P2 and P5 hyperbolas are demarked around 200 and 250 samples, being clearly visible when compared with their corresponding slices in Figure 4.1a. In slice P3 a slightly demarked hyperbola can be located around 200 and 250 samples and, over it, a bigger hyperbola that contains the former; this is due to the anomaly produced by the presence of water leaking out of the pipe. Slice P4 shows a hyperbola between 200 and 250 samples and, to its right, a couple of hyperbolas, which were also present in Figure 4.1a; the difference now is that in slice P4 of Figure 4.3a it is possible to detect a thin hyperbola over the couple of hyperbolas detected previously, this suggesting the presence of water. Also the hyperbolas caused by the pipe show a distortion due to the water leaking out of the pipe.

In Figure 4.3b the slices obtained after the variance filter are shown. The filter casts new relevant results, allowing obtaining previously not visible characteristics when compared with raw slices. The first slice, P1, shows clearly the hose that allows water to enter the system. The hose is located vertically around 150 to 225 samples approximately and, next to it, a circular shape is demarked. The circular shape corresponds to the pipe and it is located between samples 225 and 300; the same occurs in slice P6 for water leaving the tank. In slices P2 and P5 a well defined ensemble of 3 hyperbolas can be identified; this shows the water contained in the pipe. Slices P3 and P4 denote the presence of water leaking; to the left

the shapes that belong to the pipe and to the right the shapes that belong to the zone where the leak is located can be observed.

Finally, Figure 4.3c shows the binarized images, as well as the shapes and boundaries selected that match the pipe and the leak.

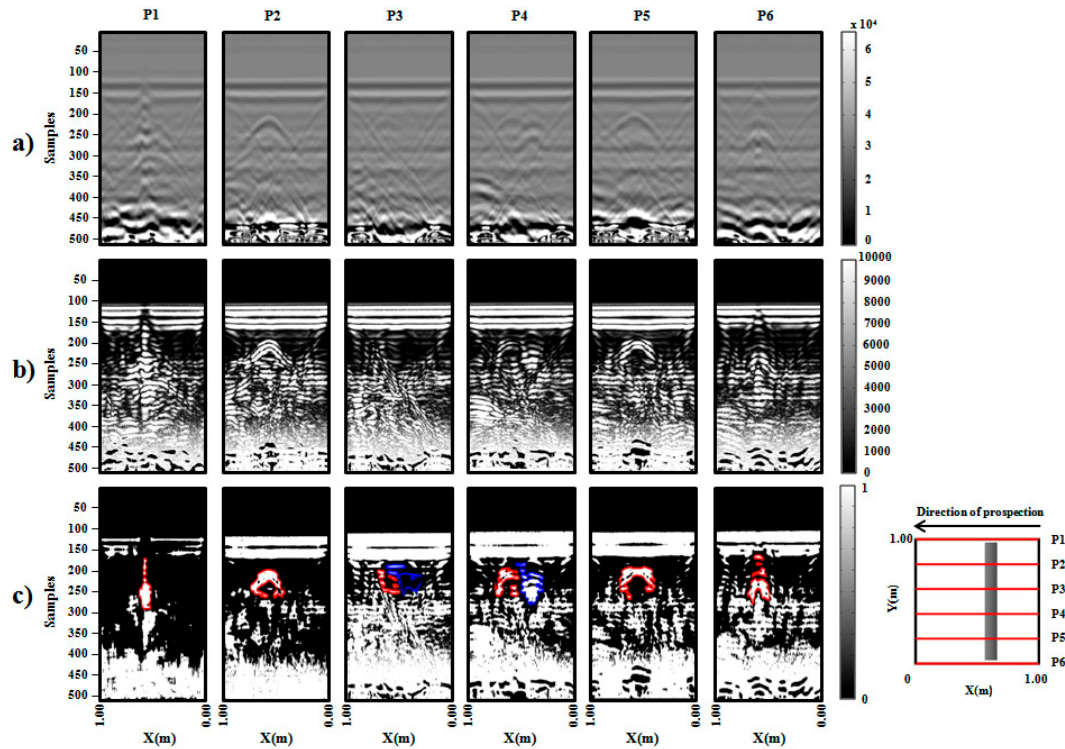


Figure 4.3 a) Raw images, b) variance filter images, and c) binarized images

4.4. Second scenario – Longitudinal slices

The raw longitudinal slices for this scenario are shown in Figure 4.4a. We remember that these slices were taken with a leak present in the system. In slice P3 a slight perturbation in the shape of a hyperbola located around 200 samples depth approximately is observed. Also, in slice P4, two parallel lines that correspond to the pipe can be seen; these lines are cut in the middle of the image and join together to form an X, and, over it, a hyperbola is located showing the presence of the leak. The precise location of the leak, as well as the wet area around the leak can also be detected. Figure 4.4b shows the images resulting of applying the variance filter; in this figure, the visualization of the pipe and the leak is clearer than before: slice P3 has a dark mark between samples 175 and 250 and fits the observed wet soil caused by water leaking out of the pipe. Slice P4 shows the pipe filled with water; it is now clearer than before to observe the area were the leak is located, the reach of the leak, and the pipe itself. The pipe is located between samples 200 and 250, and the wet zone (affected by the leak) is easily identifiable in the center of the image between samples 125 and 275. Finally, Figure 4.4c shows the binarized slices as well as the respective boundaries of the objects.

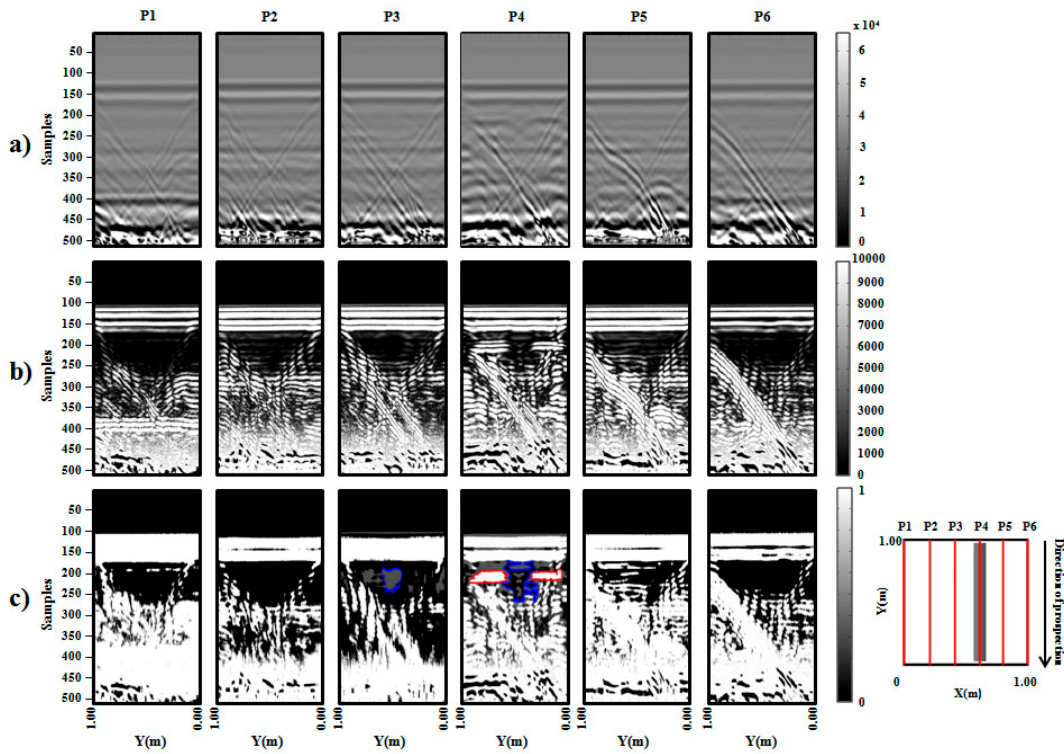


Figure 4.4 a) Raw images, b) variance filter images, and c) binarized images

The previously shown images show relevant information that allows locating the pipe and the anomalies present in the GPR images, a leak in our case. The variance filter provides an easy way to detect, locate and extract characteristics of the images.

5. COMPARISON ANALYSIS USING A MULTI-AGENT BASED METHOD

In this section, a comparison analysis between the obtained results using the variance filter and the MABS preprocessing algorithm is presented. The final objective is to highlight each method characteristics, which help GPR image analysis, making it easier the visualization and identification of anomalies in the images, in a clearer and easier way. To this aim, the basic principles of the algorithm are shown, as well as a comparison analysis between the obtained images with each method.

5.1 Pre-processing algorithm with multi-agent systems

The pre-processing of GPR images used in this section was proposed by Ayala-Cabrera et al. (2013b) and was termed an *agent race*. The algorithm is developed in Matlab, is based on game theory and uses the multi-agent paradigm (Shoham et al., 2009). The input to this algorithm is the raw GPR image (radargram) of the GPR prospection, which consists of an $m \times n$ -sized matrix. The n traces, of length m , that are generated are used in this work as parallel tracks for the n -agents to run. The race is an endurance test for the competing agents, the prize for each agent being a movement step for each effort performed. Those efforts are based on wave amplitude value changes in each column of the matrix (radargram). The agent

race includes two phases: a) warming-up and b) competition. The race takes a total time $tt = tw + tr = m$, tw being the warming-up time and tr the competition time. The displacements of the agents during time tr are conditioned by the trend change of the wave amplitude on the trace that is being run. The race ends when time tt has elapsed, and the race winner is the agent who has obtained the largest displacement during this time. The output (output A) of this process consists of an $m1 \times n$ matrix, $m1$ being the maximum number of displacements. Columns in this matrix describe the movement of the agents related to the competition. In this work, the movements obtained by the agents are called time lines. On each time line, the time obtained in the competition by each agent is sorted by increasing values, indexed from 1 on, giving equal indexes to equal times. These time lines are later normalized, obtaining Output B, which is the matrix used to compare later on. Figure 5.1 shows visually the latter.

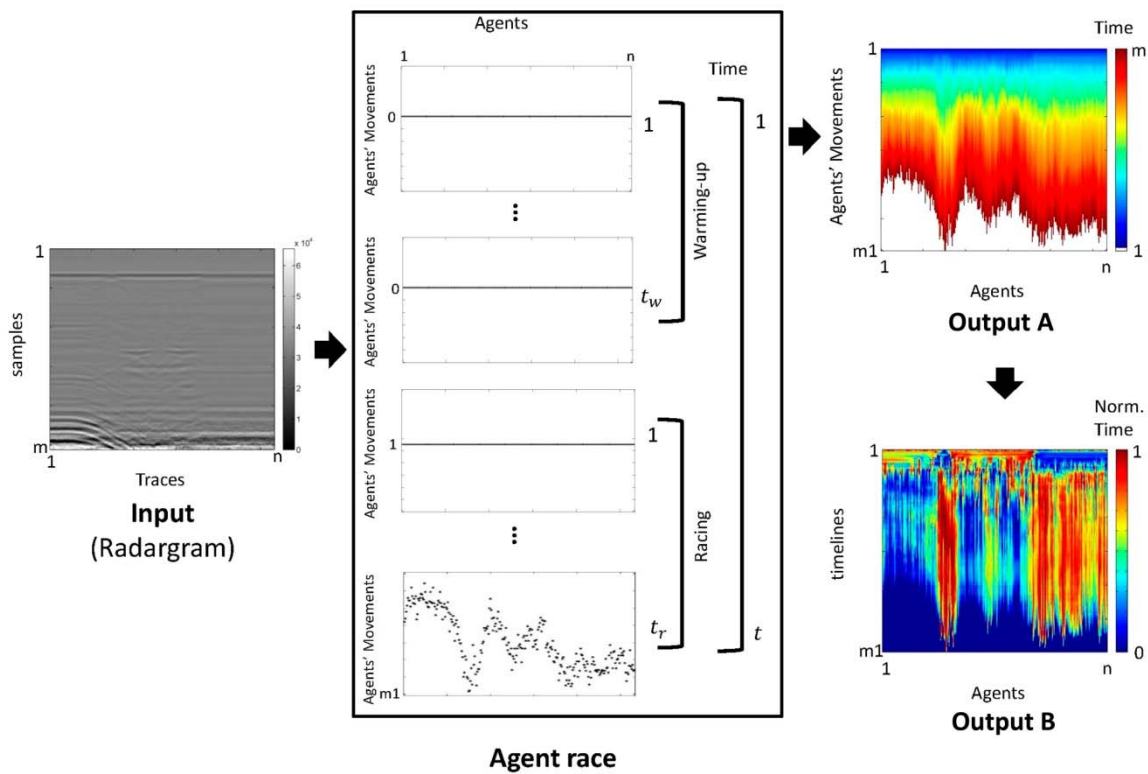


Figure 5.1 Scheme for the agent-race algorithm (Ayala-Cabrera et al., 2013b)

5.2 Comparison and image analysis

In the following sub-paragraphs, the comparisons between the variance filter and MABS resulting images presented. For the first scenario (subsections 5.2.1 and 5.2.2), transversal and longitudinal slices are shown in Figures 5.2 and 5.3 respectively. Additionally, for the second scenario (subsections 5.2.3 and 5.2.4), the transversal and longitudinal slices for both methods are shown in Figures 5.4 and 5.5.

5.2.1 First scenario comparison - Transversal slices

Figure 5.2a shows the slices using the MABS algorithm. In the slices, it is possible to observe the presence of an elliptic formation between time lines 10 and 20 and between 0.5 and 0.6m in the sense of the x axis; the presence of this elliptical formation corresponds approximately to the place where the PVC pipe is buried. Additionally, the color intensity of the ellipse is stronger in the center of the ellipse and vanishes close to its border; this characteristic favors the location of the pipe. Moreover, slices P1a and P6a show additional formation above the ellipse: the shape of the formation is triangular and is located at time line 5 approximately; this corresponds to the input and output hoses. This has to be highlighted since this formation is not easily detected in the variance filter processed slices (b). However, in contrast, in the variance filter processed slices it is easier to locate the pipe. The shapes obtained with each method are different. The pipe shape is identified by ensembles of hyperbolas in the variance filter slices (b), while in the MABS (a) the pipe is shown by ellipses. Nonetheless, the difficulty in identifying and locating shapes in the slices (a) is harder because the image composition produces some confusion among shapes in the slice.

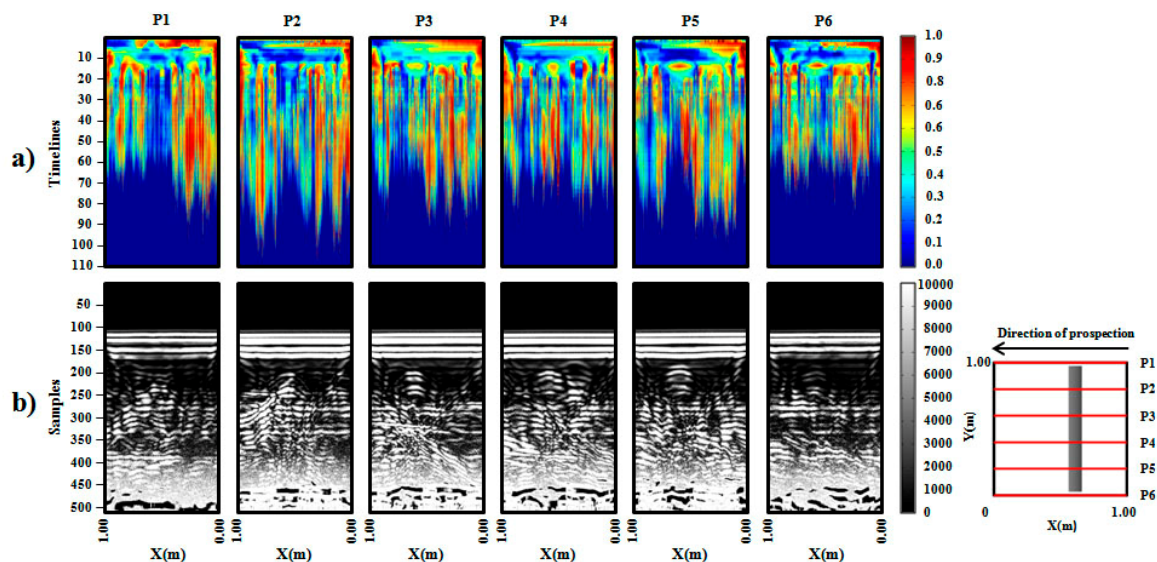


Figure 5.2. (a) MABS pre-processed images and (b) variance filter images

5.2.2 First scenario comparison - Longitudinal slices

Figure 5.3 shows the slices longitudinal to the pipe. Focusing first on the slices (a), it can be observed that each slice is different, but nothing particular can be seen at first look. However, if a detailed analysis is performed, in slice P4a, between time lines 10 and 20, intense yellow linear formations can be seen that are not present in any other slice. This formation corresponds to the upper and lower boundaries of the buried pipe. In contrast, focusing now on slices (b), it is possible to identify with certain ease the pipe in slice P4b; this is because the high variance value allows this zone to be brighter, improving a fast pipe location.

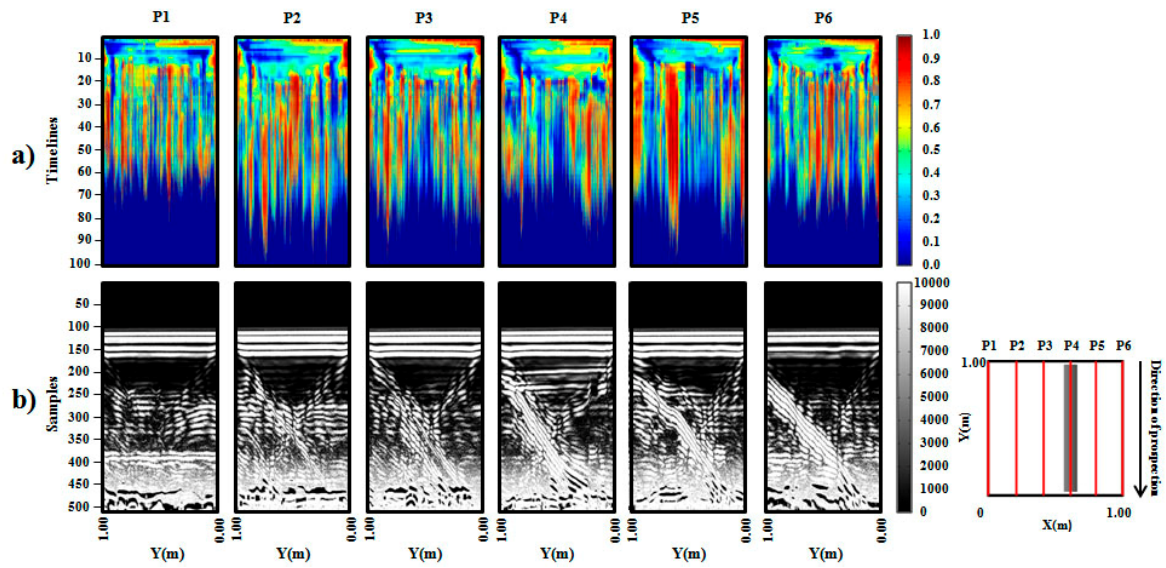


Figure 5.3. (a) MABS pre-processed images and (b) variance filter images

5.2.3 Second scenario comparison - Transversal slices

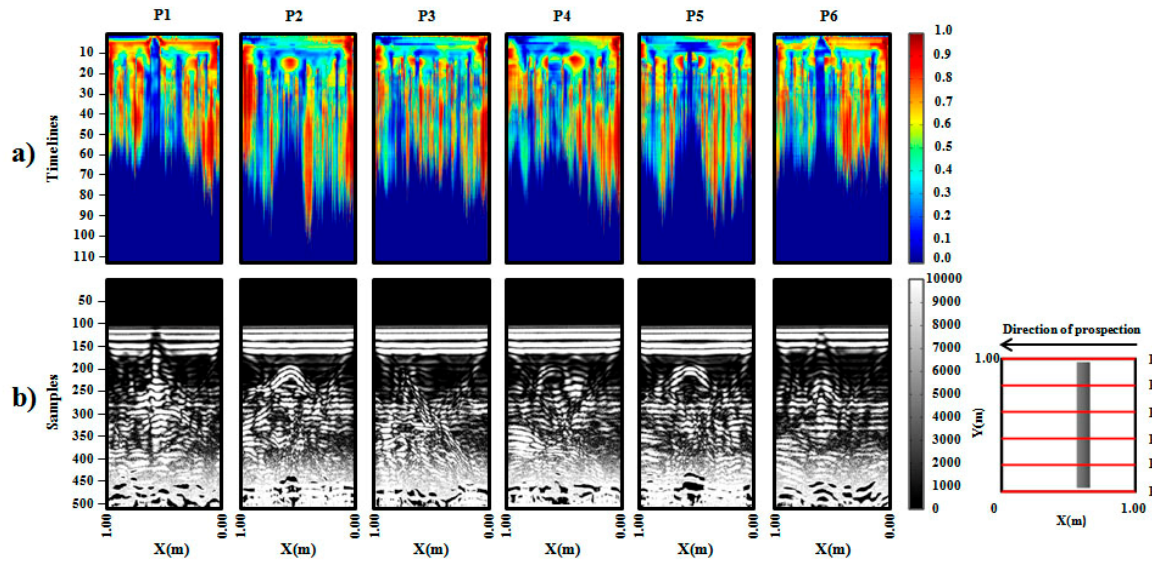


Figure 5.4. (a) MABS pre-processed images and (b) Variance filter images

Figure 5.4 shows the transversal slices of the second scenario, a scenario in which the pipe is leaking. By analyzing the slices in figure 5.4a, it is observable that the ellipse previously detected in the Figure 5.2a has higher color intensity because of the water present in the system.

In figure 5.4b it is possible to observe that the hyperbolas are closer and tighter between them, changing its shape slightly when comparing with the slices shown in Figure 5.2b.

In figure 5.4, in slices P1a and P6a, the input hose and the output hose, respectively, can be observed as an increase of color intensity because of the water passing through. When compared with slices P1b and P6b, the hose is shown connected to the main PVC pipe as an

ensemble of hyperbolas, improving the image analysis, as it reflects how it is connected in reality.

Finally, slices P3a and P4a show an ellipse of lower color intensity (blue) over the ellipses identified as the pipe; this matches the wet area caused by the leak, showing that the leak is above the buried pipe. Opposite to those slices, slices (b), especially P3b and P4b show that the wet area extends through the right to the top of the buried pipe.

5.2.4 Second scenario comparison - Longitudinal slices

In Figure 5.5, the longitudinal slices that show the water leaking out of the pipe are presented. Starting with the analysis of slices (a), the characteristics of these slices are very different as well as the color intensity. However, looking closer to slices P3a and P4a, it is possible to highlight ellipses appearing between time lines 5 and 15, the biggest being the ellipse of slice P4a, which matches where the leak is located. Slices (b) allow identifying easily the zones affected by the leak, which are shown in slices P3b and P4b. Additionally, slices (b) favor the visualization of the pipe itself; this helps the accurate location of the leak.

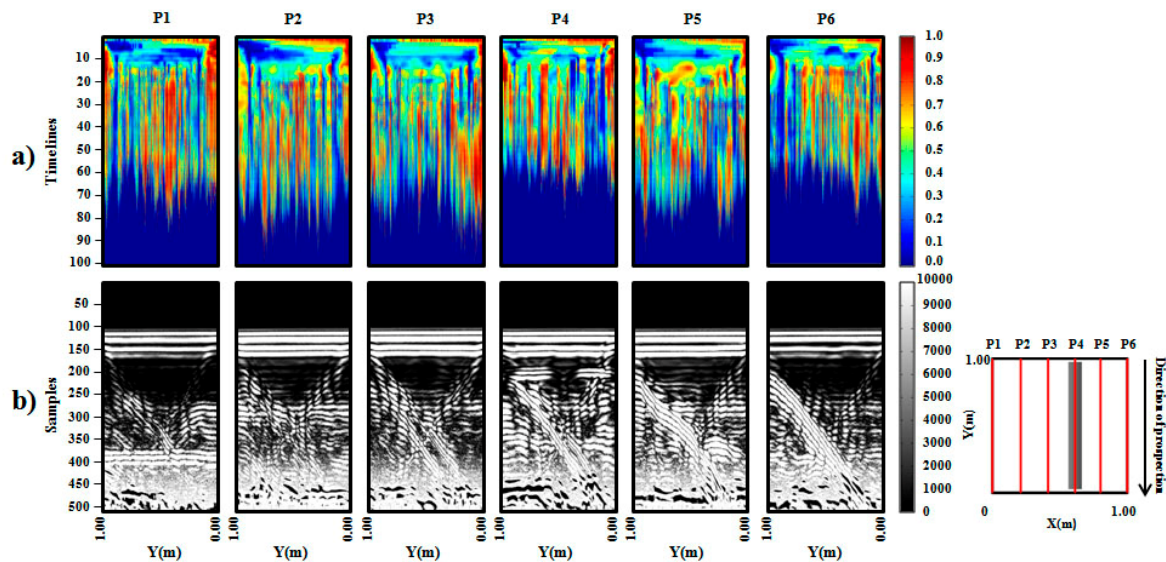


Figure 5.5. (a) MABS pre-processed images and (b) variance filter images

Finally, from this comparison analysis, we can conclude that both methods are efficient, easily applicable, and allow extracting buried pipe characteristics and also anomalies present underground, such as water leaks. The MABS algorithm favors to obtain shapes that are similar to the pipe shape, but has an inherent difficulty because of image composition and colors. This may introduce confusion when interpretation is done. And even more, if the studied area composition is unknown, misinterpretation can occur with relatively ease. In its turn, variance filtering has an advantage over the previously mentioned method, because variance filtering allows highlighting pipe characteristics or leaks making them visible at first look, being also easily identifiable. Other advantage is that the pipe can be located transversally (usual appearance of hyperbolas) or longitudinally. Finally, the slices processed using the variance filter reduce confusion because the contrast between values can highlight

better some characteristics. For example, higher values correspond to brighter areas (pipe), while lower values are darker on the image (leak).

It must be stated clearly that this work has been developed under controlled laboratory conditions, which benefits feature identification.

6. 3D MODEL COMPARISON

Various techniques are used in GPR subsurface target reconstruction (Zhou et al., 2016). In this section, a 3D model is created to improve comprehension and visualization of the results of both methods. The 3D model is built by merging contours, first placing the extracted contours in their corresponding slice spatial coordinates and then applying Matlab3D *delaunay* function (Matlab, 2012), which creates a 2-D Delaunay triangulation of the points (x,y) , where x and y are column-vectors. The procedure is analogue as the one shown by Ayala-Cabrera et al. (2014).

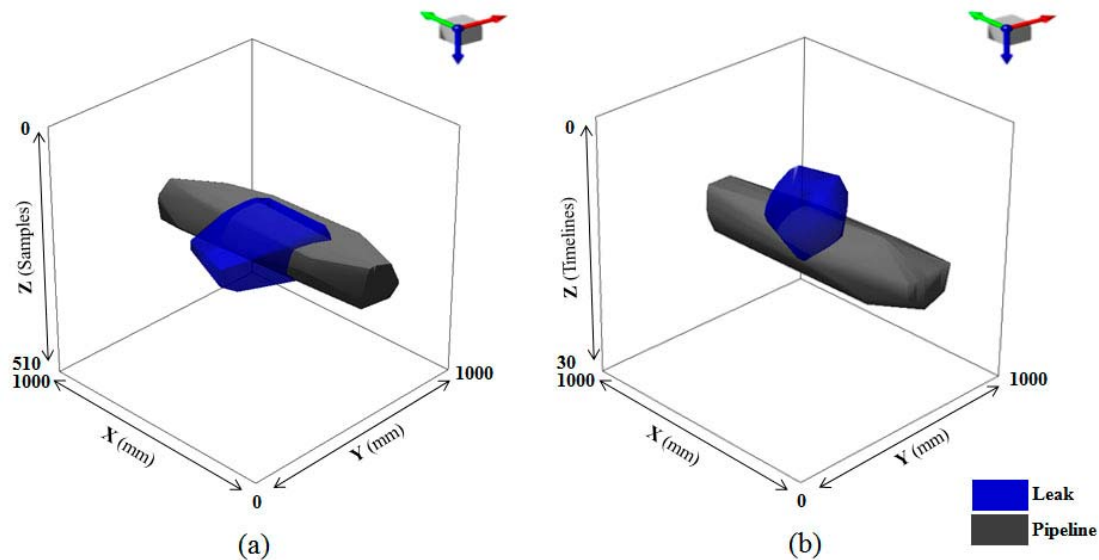


Figure 6.1. 3D Models: (a) 3D model obtained from variance filter images and (b) 3D model obtained from MABS pre-processed images

To complete the comparison between both methods, Figure 6.1 shows the 3D models obtained from each method. Figure 6.1a shows the 3D model obtained from the images after application of the variance filter, and Figure 6.1b is the 3D model from the MABS pre-processed images. By comparing both models, a slight difference can be noticed. It can be observed that in Figure 6.1b the pipe is rounder than the one in Figure 6.1a. This is because of the elliptical shapes found in the MABS pre-processed images, favoring a shape that is more similar to the real pipe. Also there is a big difference when looking at the wet area volume of each model. Figure 6.1a has a wider and scattered shape moving away from the pipe to the X axis; in contrast, Figure 6.1b shows a more concentrated volume located over the pipe.

Finally, in spite of the differences, both models are very approximate to the reality because both allow locating the leak precisely. We have to observe, however, that a suitable 3D representation depends on the correct interpretation and the forms found in the GPR images.

7. CONCLUSIONS

GPR is a potentially powerful tool to obtain valuable information for the location of leaks in water supply systems. This document applies a methodology based on a variance filter to facilitate the display of features that are not reflected in the raw images, thus facilitating the interpretation work for non-highly skilled personnel in GPR data handling.

The benefits of this process are the following. First, the variance filter is an easy-to-apply filter that produces images that help identify the contrast between the different materials present in the image and the objects that are being studied. This improves a precise location of the leak, and also the extraction of contours corresponding to the wet zone caused by water leakage. Also the pipe is easily located. Using this information, it is possible to create 3D models to help visualize and understand the phenomenon. Additionally, this filter allows locating the pipe irrespective of the direction (transverse or longitudinal) it is located with respect to the GPR prospection, while in other methods this is not so obvious.

Moreover, a comparison with a the MABS method for GPR image analysis is performed. This method is also used for leak identification over the images by close examination of the shapes that produces. The MABS has the ability to show elliptical shapes that are similar to the buried pipe, in places where the variance filter shows an ensemble of hyperbolas, that altogether has a circular shape. The MABS detects the input and output hoses as well as the variance filter, but the way to show the hose is different: for the MABS technique, a triangular shape, and for the variance filter, a long and thin succession of hyperbolas. However, the image composition of the MABS method may cause confusion and trigger inaccurate conclusions if not suitably interpreted. Even so, if both methods are used together, richer information can be obtained from a single GPR image, as in the case of detection of a leak and its behavior.

When compared both 3D models, the MABS algorithm shows a rounder shape, but the leak is more consistent in the variance filter 3D model. However, in contrast, the pipe form is not as round as in MABS. In both cases, pipe and leak can be clearly shown.

Finally, the contours obtained in this process are intended to serve as a basis for training intelligent data classification systems that are able to detect the contours automatically and allow the ultimate objective of generating models that facilitate the understanding of leaks in WSSs. The authors are currently working in this line of research.

ACKNOWLEDGEMENTS

Part of this work has been developed under the support of Fundación Carolina PhD and short-term scholarship program for the first author.

8. REFERENCES

- Atef A., Zayed T., Hawari A., Khader M., Moselhi O., 2016. Multi-tier method using infrared photography and GPR to detect and locate water leaks. *J. Autom. Constr.* 61, 162-170. <http://dx.doi.org/10.1016/j.autcon.2015.10.006>
- Ayala-Cabrera D., Izquierdo J., Ocana-Levario S.J., Perez-García R., 2014. 3D Model Construction of Water Supply System Pipes Based on GPR Images. *Proc. of 7th International Congress on Environmental Modelling and Software*, San Diego, CA, USA
- Ayala-Cabrera D., Herrera M., Izquierdo J., Ocaña-Levario S.J., Perez-García R., 2013a. GPR-Based Water Leak Models in Water Distribution Systems. *Sensors*, 13, 15912-15936. <http://dx.doi.org/10.3390/s131215912>
- Ayala-Cabrera, D., Izquierdo, J., Montalvo, I., Pérez-García, R., 2013b. Water Supply System Component Evaluation from GPR Radargrams Using a Multi-agent Approach. *Math. Comput. Model.* 57, 1927-1932. <http://dx.doi.org/10.1016/j.mcm.2011.12.034>
- Ayala-Cabrera, D., Herrera, M., Izquierdo, J., Pérez-García, R., 2011. Location of Buried Plastic Pipes Using Multi-Agent Support Based on GPR Images. *J. Appl. Geophys.* 75, 679-686. <http://dx.doi.org/10.1016/j.jappgeo.2011.09.024>
- Belotti, V., Dell'Acqua, F., Gamba, P., 2002. Denoising and hyperbola recognition in GPR data. *Proc. SPIE 4541, VII Image and Signal Processing for Remote Sensing*, Toulouse, France. <http://dx.doi.org/10.1117/12.454141>
- Brennan, M.J., Joseph, P.F., Muggleton, J.M., Gao Y., 2008. Some Recent Research Results on the use of Acoustic Methods to Detect Water Leaks in Buried Plastic Water Pipes. *Institute of Sound and Vibration Research, University of Southampton*, 1-7.
- Crocco, L., Soldovieri, F., Millington, T., Cassidy, N.J., 2010. Bistatic Tomographic GPR Imaging for Incipient Pipeline Leakage Evaluation. *Prog. Electromagn. Res.* 101, 307-321. <http://dx.doi.org/10.2528/PIER09122206>
- Demerci, S., Yigit, E., Eskidemir, I.H., Ozdemir, H., 2012. Ground Penetrating Radar Imaging of Water Leaks from Buried Pipes Based on Back-Projection Method. *NDT&E Int.* 47, 35-42. <http://dx.doi.org/10.1016/j.ndteint.2011.12.008>
- Dong L., Carnalla S., Shinozuka M., 2012. GPR survey for pipe leakage detection: experimental and analytical study. *Proc. SPIE 8347, Nondestructive Characterization for Composite Materials, Aerospace Engineering, Civil Infrastructure, and Homeland Security*, San Diego, USA. <http://dx.doi.org/10.1117/12.917407>
- Fabijarińska, A., 2011. Variance Filter for Edge Detection and Edge-Based Image Segmentation. *Proc. of 7th International Conference of Perspective Technologies and Methods in MEMS Design (MEMSTECH)*, Zakarpattya, Ukraine.
- Fahmy, M., Moselhi, O., 2010. Automated detection and location of leaks in water mains using infrared photography. *J. Perform. Constr. Facil.*, 24, 242-248. [https://doi.org/10.1061/\(asce\)cf.1943-5509.0000094](https://doi.org/10.1061/(asce)cf.1943-5509.0000094)
- Gerlitz, K., Knoll, M.D., Cross, G.M., Luzitano, R.D., Knight, R., 1993. Processing Ground Penetrating Radar Data to Improve Resolution Of Near Surface Targets. *Proc. of the 6th Symposium on the Application of Geophysics to Engineering and Environmental Problems*, San Diego, USA. <http://dx.doi.org/10.4133/1.2922036>
- Gonzalez, R.C., Woods, R.E., Eddins, S.L., 2004. *Digital Image Processing using Matlab*, Pearson-Prentice Hall, New Jersey.
- Harrison, D., 2005. Threshold estimation using wavelets and curvelets on ground penetrating radar data for noise and clutter suppression. *Master Thesis, University of British Columbia, South Dakota, USA*.
- Hasan, A.E., 2012. The Use of Ground Penetrating Radar with a Frequency 1 GHz to Detect Water Leaks from Pipelines. *Proc. of the 16th International Water Technology Conference*. Istanbul, Turkey.
- Hong, W.-T., Kang, S., Lee, S.J., Lee, J.-S., 2018. Analyses of GPR signals for characterization of ground conditions in urban areas, *J. Appl. Geophys.* 152, 65-76. <https://doi.org/10.1016/j.jappgeo.2018.03.005>
- Hunaidi, O., Wang, A., Bracken, M., Gambino, T., Fricke, C., 2004. Acoustic Methods for Locating Leaks in Municipal Water Pipe Networks. *Proc. of the International Conference on Water Demand Management, Dead Sea, Jordan*.
- Hyun, S-Y., Jo, Y-S., Oh, H-C., Kim, S-Y., Kim, Y-S., 2007. The Laboratory Scaled-Down Model of a Ground-Penetrating Radar for Leak Detection of Water Pipes. *Meas. Sci. Technol.* 18, 2791-2799. <http://dx.doi.org/10.1088/0957-0233/18/9/008>
- Juliano, T.M., Meegoda, J.N., Watts, D.J., 2013. Acoustic emission leak detection on a metal pipeline buried in sandy soil. *J. Pipeline Syst. Eng. Pract.* 4, 149-155. [http://dx.doi.org/10.1061/\(asce\)ps.1949-1204.0000134](http://dx.doi.org/10.1061/(asce)ps.1949-1204.0000134)
- Lai, W.W.L., Chang, R.K.W., Sham, J.F.C., Pang, K., 2016. Perturbation Mapping of Water Leak in Buried Water Pipes Via Laboratory Validation Experiments with High-Frequency Ground Penetrating Radar (GPR). *Tunn. Undergr. Sp. Tech.* 52, 157-167. <http://dx.doi.org/10.1016/j.tust.2015.10.017>

- Lai, W.W.L., Chang, R.K.W., Sham, J.F.C., 2018. A blind test of nondestructive underground void detection by ground penetrating radar (GPR), *J. Appl. Geophys.* 149, 10-17. <https://doi.org/10.1016/j.jappgeo.2017.12.010>
- Lee, B., Oh, S., 2018. Modified electrical survey for effective leakage detection at concrete hydraulic facilities, *J. Appl. Geophys.* 149, 114-130. <https://doi.org/10.1016/j.jappgeo.2017.08.006>
- Martini, A., Troncossi, M., Rivola, A., 2015. Automatic Leak Detection in Buried Plastic Pipes of Water Supply Networks by Means of Vibration Measurements. *Shock Vib.* 2015, 1-13. <http://dx.doi.org/10.1155/2015/165304>
- Nagashree, R.N., Aswini, N., Dyana, A., Srinivas, C.H., 2014. Detection and classification of ground penetrating radar image using textural features. *Proc. of International Conference on Advances in Electronics, Computers and Communications, Bangalore, India.* <http://dx.doi.org/10.1109/ICAEECC.2014.7002403>
- Nasirian, A., Maghrebi, M.F., Yazdani, S., 2013. Leakage Detection in Water Distribution Network Based on a New Heuristic Genetic Algorithm Model. *J. Water Resour. Prot.* 5, 294-303. <http://dx.doi.org/10.4236/jwarp.2013.53030>
- Ocaña-Levario, S.J., 2014. Reconocimiento de Patrones para Identificación de Tuberías Enterradas en Sistemas de Abastecimiento de Agua a partir de Imágenes de GPR. Master Thesis. Polytechnic University of Valencia. Valencia, Spain.
- Ocaña-Levario, S.J., Ayala-Cabrera, D., Izquierdo, J., Pérez-García, R., 2015. 3D Model Evolution of a Leak Based on GPR Image Interpretation. *Water Sci. Technol: Water Supply.* 15, 1312-1319. <http://dx.doi.org/10.2166/ws.2015.093>
- MATLAB and Statistics Toolbox Release 2012b, 2012. The MathWorks, Inc., Natick, Massachusetts, United States.
- Pratt, W.K. 2007. *Digital Image Processing*, fourth ed. Hoboken, New Jersey.
- Santos, V.R.N., Teixeira, F.L., 2017. Application of time-reversal-based processing techniques to enhance detection of GPR targets, *J. Appl. Geophys.* 146, 80-94. <https://doi.org/10.1016/j.jappgeo.2017.09.004>
- Sarwas, G., Skoneczny, S., 2015. Object Localization and Detection Using Variance Filter. *Proc. of the 6th Image Processing and Communications Challenges.* Bydgoszcz, Poland. http://dx.doi.org/10.1007/978-3-319-10662-5_24
- Shaikh, S.A., Tian, G., Shi, Z., Zhao, W., Junejo, S.A., 2018. Frequency band adjustment match filtering based on variable frequency GPR antennas pairing scheme for shallow subsurface investigations, *J. Appl. Geophys.* 149, 42-51. <https://doi.org/10.1016/j.jappgeo.2017.12.013>
- Shoham, Y., Leyton-Brown, K., 2009. *Multiagent Systems: Algorithmic, Game-Theoretic and Logical Foundations*, Cambridge University Press, New York. <http://dx.doi.org/10.1145/1753171.1753181>
- Simi, A., Bracciali, S., Manacorda, G., 2008. Hough Transform Based Automatic Pipe Detection for Array GPR: Algorithm Development and On-site Test. *Proc. of Radar Conference.* Rome, Italy. <http://dx.doi.org/10.1109/RADAR.2008.4720763>
- Singh, N.P., Nene, M.J., 2013. Buried object detection and analysis of GPR images: using neural network and curve fitting. *Proc. of International Conference on Microelectronics, Communications and Renewable Energy, Kanjirapally, India.* <http://dx.doi.org/10.1109/AICERA-ICMiCR.2013.6576024>
- Stampolidis, A., Soupios, P., Vallianatos, F., 2003. Detection of Leaks in Buried Plastic Water Distribution Pipes in Urban Places - A Case of Study. *Proc. of the 2nd International Workshop on Advanced Ground Penetrating Radar.* Delft, Netherlands. <http://dx.doi.org/10.1109/AGPR.2003.1207303>
- Tavera, M., 2008. *Aplicación de Georadar para la Mejora del Rendimiento de una Red Hídrica.* Tesis de máster. Universidad Politécnica de Valencia. Valencia, España.
- Thomson, J, Wang, L., Royer, M., 2009. State of technology review report on condition assessment of ferrous water transmission and distribution systems. EPA United States Environmental Protection Agency, EPA/600/R-09/055. https://cfpub.epa.gov/si/si_public_record_report.cfm?dirEntryId=210089
- World Bank, 2016. Retrieved on 01/12/2017 from <http://www.worldbank.org/en/news/press-release/2016/09/01/the-world-bank-and-the-international-water-association-to-establish-a-partnership-to-reduce-water-losses>.
- Xue, W., Zhu, J., Rong, X., Huang, Y., Yang, Y., Yu, Y., 2017. The analysis of ground penetrating radar signal based on generalized S transform with parameters optimization, *J. Appl. Geophys.* 140, 75-83. <https://doi.org/10.1016/j.jappgeo.2017.03.016>
- Zhou, L., Ouyang, S., Liao, G., 2016. A novel reconstruction method based on changes in phase for subsurface large sloped dielectric target using GPR, *J. Appl. Geophys.* 134, 36-43. <https://doi.org/10.1016/j.jappgeo.2016.08.013>